Sustainable and Facile Route to Nearly Monodisperse Spherical Aggregates of CeO₂ Nanocrystals with Ionic Liquids and Their Catalytic Activities for CO Oxidation

Zhen-Xing Li,[†] Le-Le Li,[†] Quan Yuan,[†] Wei Feng,[†] Jun Xu,[†] Ling-Dong Sun,[†] Wei-Guo Song,[‡] and Chun-Hua Yan*,[†]

Beijing National Laboratory for Molecular Sciences, State Key Laboratory of Rare Earth Materials Chemistry and Applications & PKU-HKU Joint Laboratory in Rare Earth Materials and Bioinorganic Chemistry, Peking University, Beijing 100871, China, and Institute of Chemistry, Chinese Academy of Sciences (CAS), Beijing 100080, China

This article reports a novel preparation of nearly monodisperse spherical aggregates of CeO₂ nanocrystals by using ionic liquid (1-hexadecyl-3-methylimidazolium bromide, C₁₆MimBr) as both template and solvent. The products were characterized with X-ray diffraction (XRD), scanning electron microscopy (SEM), transmission electron microscopy (TEM), high-resolution TEM (HRTEM), X-ray photoelectron spectroscopy (XPS), Raman spectroscopy, UV−vis spectroscopy, FT-IR spectroscopy, and N₂ adsorption−desorption methods. The spherical aggregates, with average diameter of 100 − 150 nm, are composed of ca. 3.5 nm CeO₂ nanocrystals as building units, giving rise to three-dimensional (3D) open porous structures with high Brunauer−Emmett−Teller surface area of 119 m²·g⁻¹. Mesoporous CeO₂ with surface area up to 227 m²·g⁻¹ was prepared by simply tuning the amount of the ionic liquids. Loaded with 5 wt% CuO, both the spherical aggregates and the mesoporous CeO₂ exhibit high catalytic activities for CO conversion with 100% conversion rates at low temperature of 150 °C, suggesting potential applications in preferential oxidation (PROX) and water-gas shift reaction (WGSR). This sustainable and facile method may be extended to the preparation of other metal oxide nanoarchitectures and provides guidance for structure-controlled synthesis.

Introduction

As one of the most important functional rare earth oxides, ceria-based materials are attracting significant interest because of their wide applications in automotive three-way catalysts (TWCs), UV blocking and shielding materials, solid oxide fuel cells (SOFCs), gates for metal-oxide semiconductor devices, low-temperature water-gas shifts, gas sensors, and solar cells.[1] It is well-known that the functional performance of CeO₂ materials is influenced by morphology and nanostructure, including the size, shape, and surface/volume ratio.[2,3] For example, a blue shift in the ultraviolet absorption band of ceria nanocrystals was observed, owing to the quantum size effect.[4] The reaction of water-gas shift on gold-deposited ceria nanorods was more active than that of gold on other sharp ceria supports.[5] To enhance the catalytic activity and widespread application of CeO₂, more attention has been focused on control of the size and shape of primary particles as well as manipulation of their arrangement and aggregation structure.[6] Generally, porous CeO₂ nanostructures have apparent advantages in enhancing the catalytic activities because such structures not only possess high surface area but can also effectively transport reactant molecules to the active sites.[1b,7] A variety of chemical techniques have been applied to prepare CeO₂ nanoparticles or their network structures with high specific surface areas, such as sol−gel,[8] hydrothermal synthesis,[9] spray pyrolysis,[10] surfactant-templated synthesis,[11] coprecipitation,[12] glycine-nitrate combustion,[13] one-step template-free synthesis,[14] low-temperature hydrothermal synthesis,[15] low-temperature reflux synthesis,[16] and CNT-templated synthesis.[17] Nevertheless, most of these techniques are energy consuming, manufacture complicated, and not environmentally benign. Therefore, the preparation of nanomaterials via a simple, environmentally benign, and morphology-controlled route remains a challenge, especially in the viewpoints of "green chemistry".

As a new species of reaction media, ionic liquids (ILs) have been extensively studied owing to their unique properties such as low volatility, nonflammability, high chemical and thermal stabilities, designable structures, high ionic conductivity, and broad electrochemical windows, etc.[18] Recently, ILs have proved to be an excellent media for inorganic synthesis; in addition, they have attracted increasing attention as templates or solvents for the fabrication of nanostructured materials. ILs possess tunable solvent properties through which they can easily interact with various surface and chemical reaction environments; moreover, ILs with hydrophobic regions and high directional polarizability can form extended hydrogen bond systems in the liquid state, resulting in a highly structured self-assembly.[18−22] To date, various metallic nanoparticles, such as palladium,[19a] iridium,[19b] germanium nanoparticles,[19c] and metal oxide nanostructures[18] have been prepared with ILs. Synthesis and functionalization of gold nanoparticles in ILs is also reported, wherein the color of the gold nanoparticles is tuned by changing the anions of ILs.[20] Single crystalline Te nanorods and nanowires have been prepared through microwave-assisted synthesis in ILs.[21] Morris and co-workers demonstrated the potential of ILs as both solvent and template for fabrication of zeolitic materials.[22] With different ILs as templates, Zhou et al. prepared mesoporous silica with wormlike porous and highly ordered monolithic supermicroporous lamellar structure.[18] The same

* Corresponding authors. Fax: +86-10-6275-4179; E-mail: yan@pku.edu.cn.
† Peking University.
‡ Institute of Chemistry, CAS.
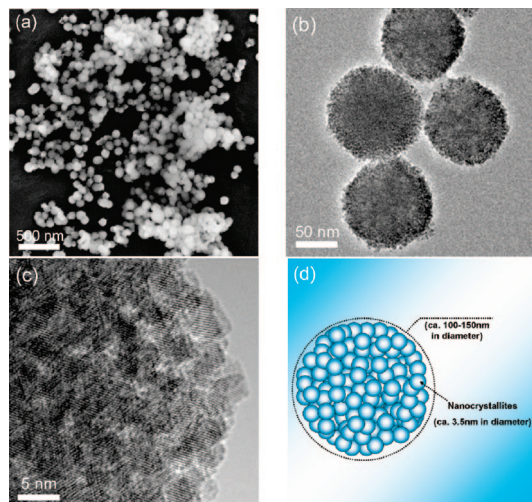
Figure 1. Morphology and structure of sample 1 prepared with 2.5 mmol ILs. (a) SEM image of the overall morphology. (b) High-magnification TEM image of individual CeO_2 aggregate. (c) HRTEM image of a typical CeO_2 aggregate. (d) A schematic diagram illustrating the microstructure of aggregated CeO_2 composed of closely packed nanocrystals.
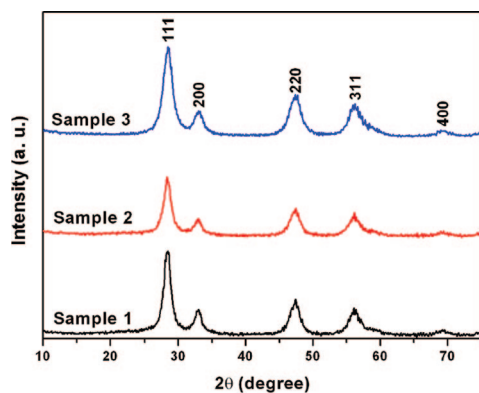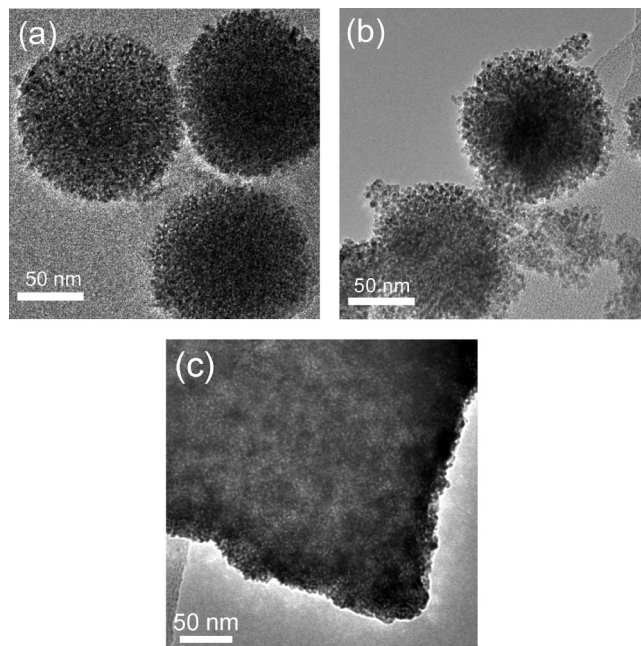

Figure 2. XRD patterns of the as-obtained CeO_2 samples synthesized with various amounts of ILs (sample 1, 2.5 mmol; sample 2, 5 mmol; sample 3, 7.5 mmol).

group also reported a mild route in ILs to fabricate 2−3 nm sized titania nanocrystals and studied their self-assembly toward mesoporous TiO_2 spheres.[18a] Most recently, Chen et al. demonstrated a novel route to prepare semiconductor ZnO nanocrystals with tunable photoluminescence and high thermal stability, which are stabilized with ILs.[23] Although some works are reported, an extensive exploration of ILs' potential in the synthesis of metal oxide nanocrystallines or their network structure has just begun.

In this work, we report a sustainable and facile synthesis of nearly monodisperse spherical aggregates of CeO_2 nanocrystals by utilizing ionic liquid (1-hexadecyl-3-methylimidazolium bromide, $C_{16}MimBr$) as both a structure-directing agent and solvent. The spherical aggregates, with an average diameter of 100−150 nm, are composed of ca. 3.5 nm CeO_2 nanocrystals

TABLE 1: Lattice Parameters (*a*) and Average Crystallite Sizes (*D*) of the CeO_2 Samples Determined by the XRD Patterns.

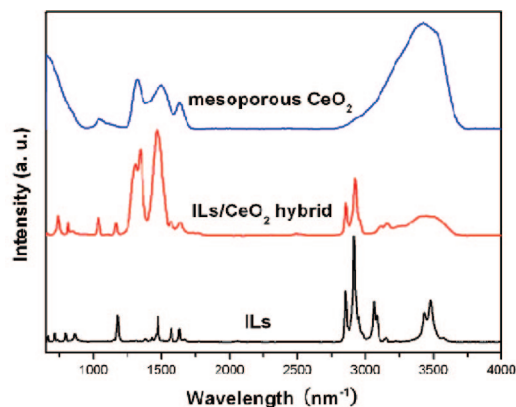| sample	lattice parameters, nm	average crystallite size, nm
1	0.5430(2)	7.0
2	0.5432(3)	6.5
3	0.5421(3)	5.4

Figure 3. TEM images showing the morphology evolution of as-obtained CeO_2 samples prepared with various amounts of ILs: (a) sample 1, (b) sample 2, (c) sample 3.
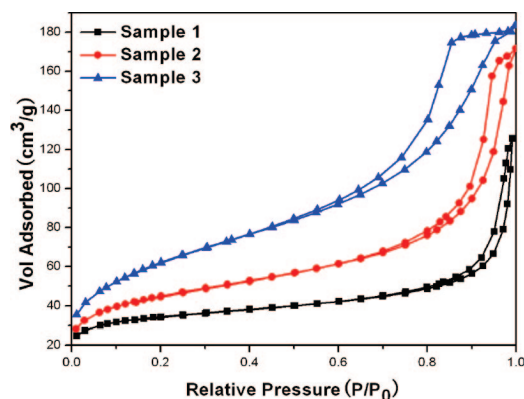
Figure 4. Nitrogen adsorption−desorption isotherms of the as-obtained CeO_2 prepared with various amounts of ILs.

Figure 5. FT-IR spectra of ILs, the ILs/CeO_2 hybrid, and mesoporous CeO_2.

as building units, giving rise to three-dimensional (3D) open porous structures with high Brunauer−Emmett−Teller (BET) surface area of 119 $m^2 \cdot g^{-1}$. Simply tuning the amount of the ILs used in the synthesis allows for the preparation of mesoporous CeO_2 with surface areas up to 227 $m^2 \cdot g^{-1}$. Loaded with

Nearly Monodisperse Spherical Aggregates

J. Phys. Chem. C, Vol. 112, No. 47, 2008 **18407**
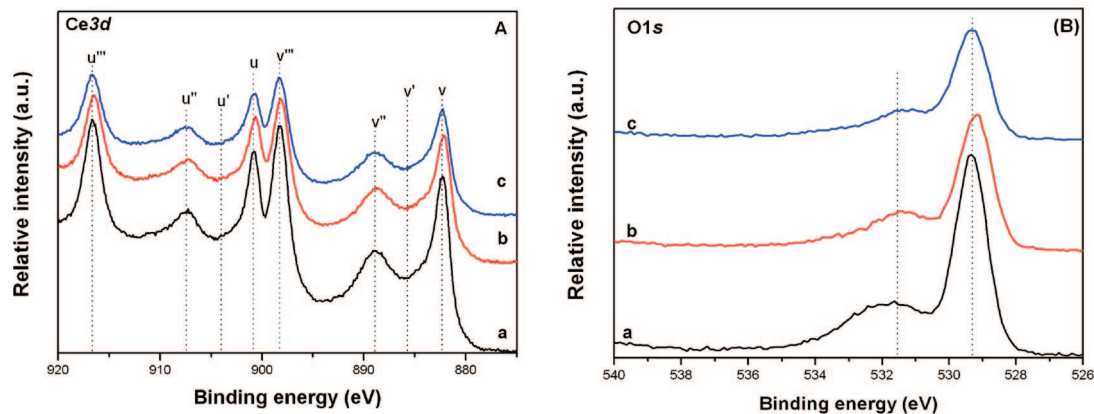
Figure 6. XPS scan survey in the region of Ce 3d (A) and O 1s (B) of the as-obtained CeO_2 prepared with various amounts of ILs: (a) sample 1, (b) sample 2, (c) sample 3.

5 wt% CuO, both the spherical aggregates and the mesoporous CeO_2 exhibit high catalytic activities for CO conversion with 100% conversion rates at a low temperature of 150 °C, suggesting potential applications in preferential oxidation (PROX) and water-gas shift reaction (WGSR).

Experimental Section

Preparation of CeO_2 Nanocrystal Aggregates. All chemicals were used as purchased without further purification. 1-Hexadecyl-3-methylimidazolium bromide (C_{16}MimBr) was prepared according to the literature method.[18f] The source of cerium $Ce(NO_3)_3 \cdot 6H_2O$ was purchased from Beijing Chemical Reagent Company.

A typical synthesis procedure is as follows. A certain amount of C_{16}MimBr (2.5, 5, or 7.5 mmol) was added in 10 mL of ethanol to form a homogeneous and transparent solution. Afterward, 5 mmol of $Ce(NO_3)_3 \cdot 6H_2O$ was added to the above solution. After vigorous agitation for 1 h at room temperature, the product was transferred to a constant temperature and humidity oven (temperature: 40 °C, relative humidity: 50%) and underwent solvent evaporation. After two days of aging, the gel product was crystallized at 100 °C for 2 days. The final precipitates were extracted with hot ethanol for 24 h. Finally, the product was annealed at 300 °C in air for 3 h at a ramping rate of 1 °C·min^{-1}. The products are denoted as samples 1 to 3 corresponding to the amount of ionic liquid used, 2.5 to 7.5 mmole, respectively.

Catalyst Preparation. Ceria-supported CuO catalyst was prepared by impregnating 155 mg of CeO_2 powder with an aqueous solution containing 24.1 mg of $Cu(NO_3)_2 \cdot 3H_2O$ (Beijing Chem. Corp. China). The suspension was stirred at room temperature to guarantee the solution soaking sufficiently into the CeO_2 powder until the water was completely evaporated. Subsequently, it was calcined at 500 °C in air for 3 h.

Characterization. X-ray powder diffraction (XRD) patterns of the samples were recorded on a Rigaku D/max-2000 X-ray powder diffractometer with Cu Kα (λ = 1.5406 Å) radiation. The lattice parameters were calculated with the least-squares method. The average crystal domain size of the ceria crystallite size (D) was estimated with the Scherrer equation:

$$D = \frac{0.90\lambda}{\beta \cos \theta}$$

where θ is the diffraction angle of the (111) peak of the cubic phase, and β is the full width at half-maximum (fwhm) of the (111) peak in radian, which is calibrated from high purity silicon. SEM observations were carried out with a DB-235 focused ion

beam (FIB) system operated at an acceleration voltage of 15 kV. TEM images were taken on a Hitachi H-9000 NAR transmission electron microscope under a working voltage of 300 kV. High-resolution TEM (HRTEM) was performed on a Philips Tecnai F30 FEG-TEM operated at 300 kV. The Raman spectra were recorded on a Jobin-Yvon LabRAM HR800 Raman spectrometer with a 30 mW Ar$^+$ laser (633.0 nm). The exposition time is 10 s and accumulates two times. X-ray photoelectron spectrometer (XPS) measurements were carried out in an ion-pumped chamber (evacuated to 2×10^{-9} Torr) of an Escalad5 spectrometer, employing Mg Kα radiation (BE = 1253.6 eV). FT-IR spectra were recorded on a Nicolet Magna-IR 750 spectrometer equipped with a Nic-Plan Microscope. The nitrogen adsorption and desorption isotherms at 78.3 K were measured on an ASAP 2010 analyzer (Micromeritics Co. Ltd.). Measurements were performed after outgassing the sample at 393 K under a vacuum, down to a residual pressure less than 10^{-3} Torr. With the Barrett–Joyner–Halenda (BJH) model, the pore volumes and pore size distributions were derived from the desorption branches of the isotherms. The UV–vis spectra of the nanocrystal dispersions were recorded on a Hitachi U-3010 spectrometer with a quartz cell (1 cm path length), and pure ethanol was used as a blank. The optical absorption coefficient α was calculated according to the following equation:

$$\alpha = (2.303 \times 10^3 A\rho)/lc$$

where A is the absorbance of a sample, ρ is the real density of CeO_2 (7.28 g cm^{-3}), l is the path length, and c is the concentration of the ceria suspensions.

CO Oxidation Test. A homemade flow reactor system including a quartz reaction tube (8 mm × 42 mm) was used for the catalytic test. In a typical CO oxidation experiment, 50 mg of CuO–CeO_2 sample and 450 mg of sea-sand were mixed as catalyst, and the experiment was carried out at 25 SCCM flows of 1% CO concentration in nitrogen and 25 SCCM air. The gas composition was monitored online on a Shimadzu GC-14C equipped with a TCD detector.

Results and Discussion

In conventional solution synthesis, the nanostructures of inorganic materials are induced with hydro/solvothermal treatment or with assistance of additional organic solvents in a sealed autoclave. In contrast, the present synthesis is developed in an open container at ambient pressure, meanwhile, ILs play a key role in the fabrication of the nanostructured CeO_2. Moreover, ILs used in the fabrication are recyclable through a simple
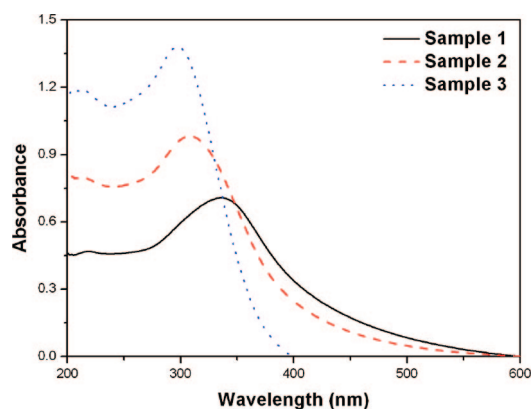
Figure 7. UV−vis spectra of the as-obtained CeO_2 prepared with various amounts of ILs.

extraction process and the extraction efficiency is higher than 90%, providing the present process with better sustainability which is very crucial for "green chemistry". The size, morphology, and structure of sample 1 prepared with 2.5 mmol ILs are measured with scanning electron microscopy (SEM) and transmission electron microscopy (TEM). SEM and TEM images of as-obtained samples are shown in Figure 1a−c. The SEM images (Figure 1a) of the CeO_2 samples are nearly monodisperse spherical aggregates with the average diameter in the range of 100−150 nm. Figure 1b shows a magnified TEM image of individual CeO_2 aggregate, revealing that the CeO_2 aggregate consists of packed small nanocrystals. The HRTEM image (Figure 1c) clearly shows that each spherical aggregate CeO_2 is composed of CeO_2 nanocrystals with a size of ca. 3.5 nm. The lattice fringes are indicative of the high crystallinity of the spherical aggregates, with an interplanar distance of 0.33 nm indexed to the (111) of cubic CeO_2 and the interplanar distance of 0.28 nm indexed to the (200) plane. The geometrical structure of an individual aggregate is further schematically illustrated in Figure 1d to demonstrate the porous features resulting from the aggregation of nanosized crystallites.

The XRD patterns of the CeO_2 samples 1−3 are illustrated in Figure 2. All the diffraction peaks for every sample can be indexed to (111), (200), (220), (311), and (400) reflections, corresponding to a face-centered cubic (*fcc*) fluorite structure with lattice constants in the range of 0.5421−0.5432 nm (JCPDS card no. 34−0394, $a = 0.5411$ nm, space group *Fm3m*). No crystallized precursor is observed in the XRD pattern, and the broadening of the reflections distinctly indicates the intrinsic nature of nanocrystals. The characteristics of the ceria samples are summarized in Table 1. With the amounts of ILs increased from 2.5 to 7.5 mmol, the average crystallite size (*D*) of ceria nanocrystals, calculated by the Sherrer formula, is reduced from 7.0 to 5.4 nm. The calculated XRD domain size is significantly smaller than the TEM size, demonstrating that the CeO_2 spherical aggregates are composed of small CeO_2 nanocrystals.[24] A closer observation of the reflection peak (111) reveals a slight downshift with the increasing ILs, indicating an increase in the unit cell volumes (Table 1).

Typical TEM images of samples 1−3 shown in Figure 3 reveal a gradual degradation in the degree of spherical aggregation of nanocrystallites and an elevation in the uniformity of the pore structure of aggregation with an increasing amount of ILs. It is obvious that the spherical morphology is destroyed gradually from sample 1 to sample 3 with an increasing amount of ILs used. When the amount of ILs increases to 7.5 mmol, no spherical aggregates are obtained, but uniformly distributed wormhole-like mesoporous structure is observed through the

whole sample with isotropic mesopores and readily accessible openings from any directions.

The surface area and porosity of the obtained CeO_2 samples are investigated with the nitrogen adsorption−desorption isotherms, as shown in Figure 4. The presence of a pronounced hysteresis loop in the isotherm curves indicates that the pores are in 3D intersection networks for all the three samples.[25] As the amount of ILs increases, the materials gradually exhibit typical type IV isotherms according to the IUPAC classification, signifying the mesoporous structure for the sample 3. As evaluated with the classical BJH model based on the analysis of desorption branch of the nitrogen adsorption isotherm, the primary mesopores measured in sample 3 are of ca. 2 nm, close to the diameter expected for a single rod micelle of ILs templates. With an increasing amount of ILs used, the BET surface areas of the mesoporous CeO_2 increase from 119 to 227 $m^2 \cdot g^{-1}$. The differences in structures and BET surface areas of the three samples are determined from the TEM images shown in Figure 3. Sample 1 is composed of a porous network of aggregated nanoparticles with a porosity arising from the interparticle space, while sample 3 shows uniformly distributed wormhole-like mesopores through the sample, which is best described as one-dimensional rod-type micelles entangled in a 3D manner. As a result, this structure provides an isotropic porous structure with easily accessible pore openings from any directions, which is highly desirable for various electrochemical and catalytic applications. It is presumed that an increasing amount of ILs would induce the stacking arrangement of its cations or anions, resulting in a supermolecular structure of ILs, and then cause an increase in surface area of the as-obtained CeO_2. The FT-IR spectra are analyzed to reveal the formation process of mesoporous ceria. Figure 5 shows the FT-IR spectra of the ILs, the ILs/CeO_2 hybrid, and mesoporous CeO_2. The strong peaks around 2851 and 2916 cm^{-1}, attributed to the alkyl chain of ILs,[26] are still present and do not shift in the spectrum of the ILs/CeO_2 hybrid. Similar to the IL-templated formation mechanism of mesoporous silica,[18d−f] the mesoporous structure of the ILs/CeO_2 hybrid is formed through hydrogen bonding between ILs and cerium hydroxide as well as $\pi-\pi$ stacking of imidazolium rings. In the spectra of ILs and the ILs/CeO_2 hybrid shown in Figure 5, the two characteristic bands of the imidazolium ring around 3062 and 3082 cm^{-1}, corresponding to the symmetric and asymmetric stretch of the C−H bond in positions four and five of the imidazolium ring,[27] are found to be considerably broadened and shifted to 3120 and 3158 cm^{-1}. These effects demonstrate a strong interaction between the imidazolium headgroup and the inorganic matrix. The proposed hydrogen-bond-co-$\pi-\pi$-stack mechanism is responsible for the formation of the wormlike framework of mesoporous materials, although it still needs further study.

The representative photoelectron peaks of Ce 3d and O 1s for the obtained samples are shown as panels A and B in Figure 6. The Ce 3d spectra exhibit the features of shakeup and shake-down processes which have been investigated in great detail.[28] The features of the Ce^{3+} initial state are labeled as u′ and v′ for $3d_{5/2}$ and $3d_{3/2}$ states, respectively, while those due to the Ce^{4+} initial state are labeled as u, u″, u‴, v, v″, and v‴, where the superscript corresponds to different final states and the v and u correspond to the $3d_{5/2}$ and $3d_{3/2}$ states, respectively. Six Ce 3d binding energy (BE) peaks are consistent with the previous report of Ce^{4+}, indicating the main valence of cerium in these samples is +4, and no apparent peaks of Ce^{3+} are observed. Panel B of Figure 6 gives the O 1s spectra of CeO_2 samples prepared with various amounts of ILs. It is noted that the spectra of the three samples consist of

Nearly Monodisperse Spherical Aggregates

J. Phys. Chem. C, Vol. 112, No. 47, 2008 **18409**
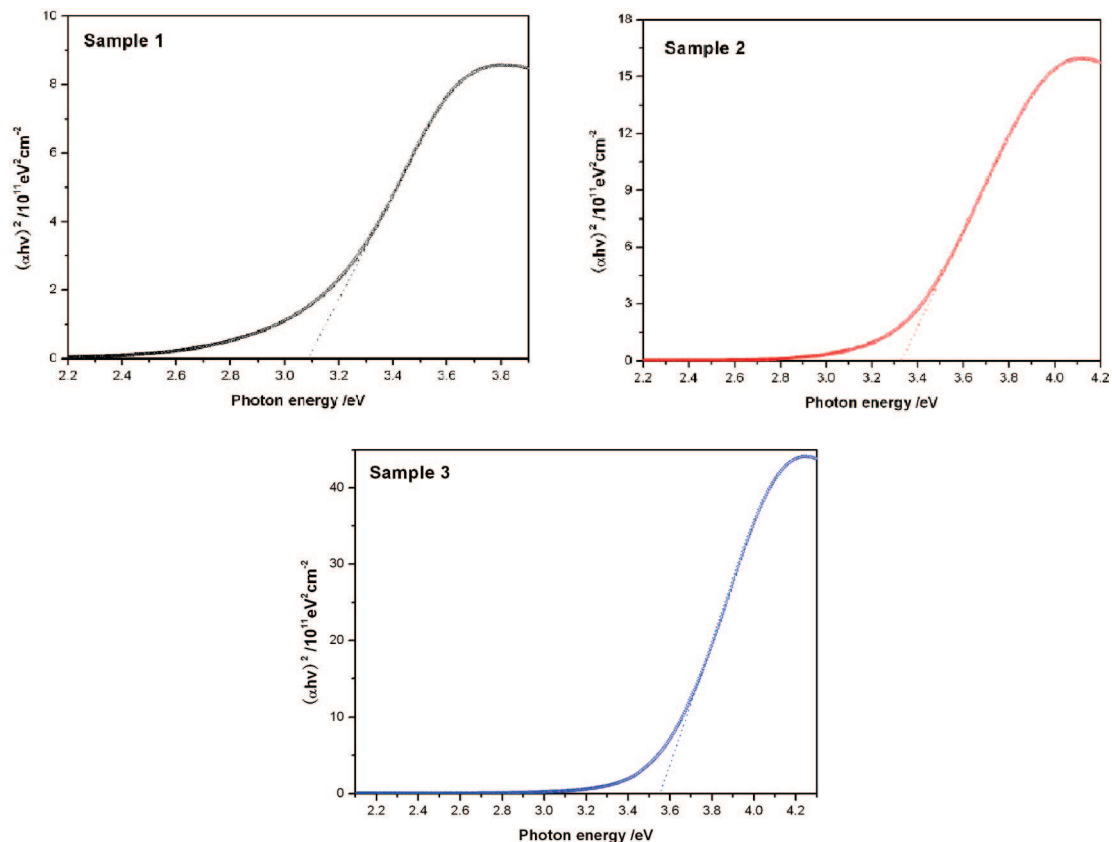
Figure 8. Plot of $(\alpha h\nu)^2$ versus photon energy of the as-obtained CeO_2 prepared with various amounts of ILs.
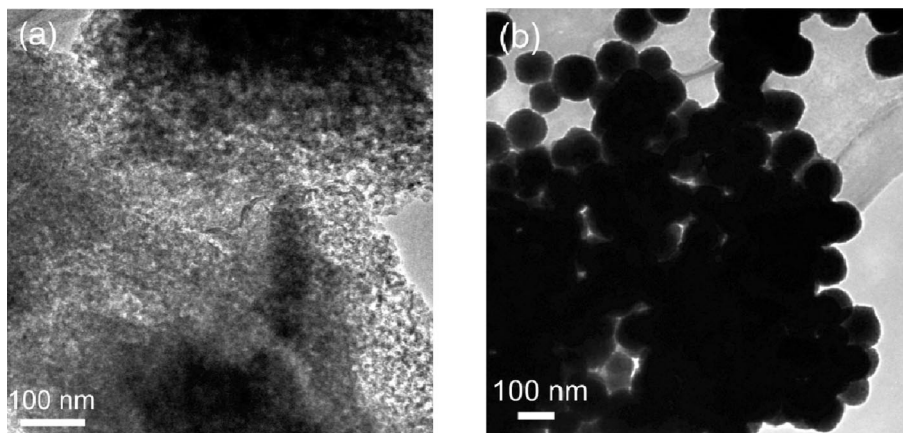

Figure 9. TEM images of the sample prepared (a) before and (b) after the thermal treatment at 100 °C.

two peaks: one at 531.6 eV, ascribed to the absorbed oxygen, and the other at a lower BE, ascribed to the lattice oxygen.[28]

To reveal the correlation between the band gap energies and the crystallite size and structure of the three samples, the UV−vis absorption spectra were recorded (Figure 7). All the samples distinctly exhibit a strong absorption band (below 400 nm in wavelength) at the UV region due to the charge-transfer transitions from O 2p to Ce 4f, which overruns the well-known f−f spin−orbit splitting of the Ce 4f state.[29] The plots of $(\alpha h\nu)^2$ vs photon energy of ceria are shown in Figure 8. For direct transitions, α near the absorption edge can be expressed in the following equation: $\alpha \propto (h\nu - E_d)^{1/2}/h\nu$, where α is the absorption coefficient, $h\nu$ is photon energy, and E_d is the band gap energy for direct transitions.[29] In the present case, the value of direct band gap energy shows a gradual increase (3.09, 3.33, and 3.55 eV for the three measured samples, respectively) as the amount of used ILs increased, which is consistent with the reduction in crystallite size. It has been

theoretically deduced that the value of blue-shifting is inversely proportional to the square of the crystallite size due to quantum confinement effect.[29c−e] This trend agrees well with the crystallite size change obtained from the Sherrer formula. Moreover, since the valence of cerium is +4 in samples 1−3 (as revealed by XPS), this blue-shift should not be attributed to Ce(III)-related effect as observed by some groups.[29d]

For the purpose of clarifying the effect of ILs on the formation of ceria spherical aggregates, the structure and morphology of ceria spherical aggregates (sample 1) after evaporation of ethanol are examined. Figure 9a shows the TEM image of the sample prepared before thermal treatment at 100 °C (denoted as sample A). No CeO_2 spherical aggregate is formed during this process. The sample prepared after thermal treatment at 100 °C and before the extraction process (denoted as sample B) clearly exhibits spherical aggregates (Figure 9b), indicating that a thermal process with assistance of ILs is the key step for the formation of ceria spherical aggregates.
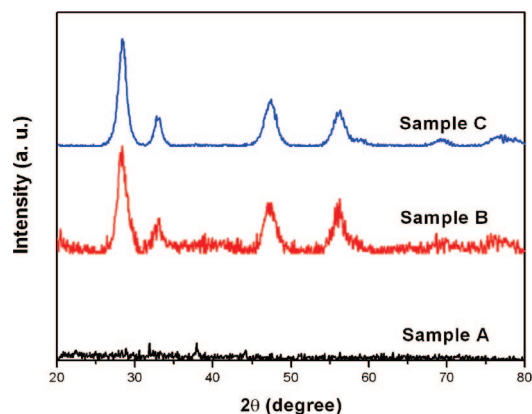
Figure 10. XRD patterns of the sample prepared before (sample A) and after (sample B) the thermal treatment at 100 °C, and spherical aggregate ceria (sample C).
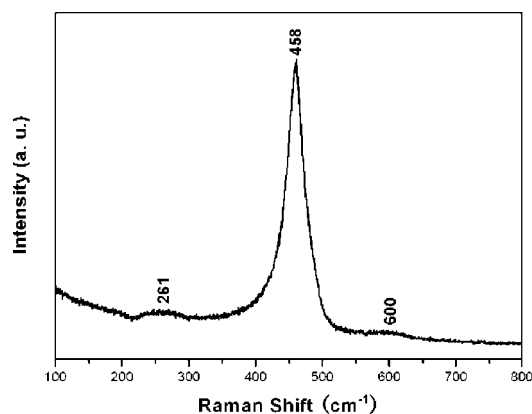
Figure 11. Raman spectra of the spherical aggregates CeO_2.
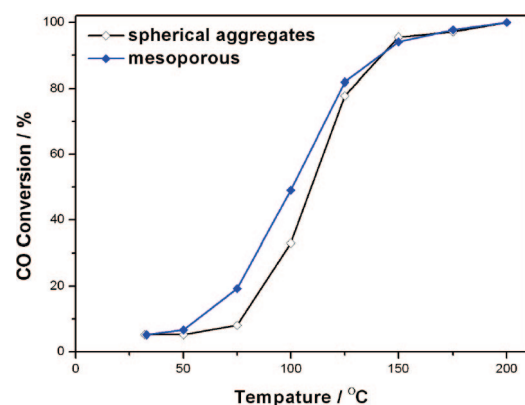
Figure 12. CO conversion as a function of temperature for spherical aggregates and mesoporous $CuO-CeO_2$ catalyst.

Most of the ethanol is evaporated and removed during the thermal process because of the volatility and low boiling point, while the ILs are not easily removed because of the thermal stability and nonvolatility. The ILs are thus proposed to act as both ionic solvents and templates during the subsequent heating for the formation of CeO_2 spherical aggregates.[30] In addition, evidence is also obtained from the analysis of the XRD patterns (Figure 10). The diffraction peaks for sample B can be exactly indexed to an *fcc*-phased ceria, whereas sample A shows no diffraction peaks corresponding to the *fcc* phase of CeO_2. On the basis of above results, it is suggested that ethanol acts as a reactant and dispersing agent which causes the cerium precursor and ILs to be mixed well, while ILs play dual roles of both template and cosolvent agents in fabricating the ceria spherical aggregates. The dual functions of ILs have been

previously demonstrated by Hong et al. in fabrication of mesoporous γ-alumina.[18g]

Figure 11 shows the typical Raman spectra of the ceria spherical aggregates. It is known that only one sharp Raman peak at 464 cm^{-1} is observed for the bulk ceria, which is assigned to F_{2g} symmetry as a symmetric breathing mode of the oxygen atoms around the cerium ions.[31] For the ceria spherical aggregates, the first-order peak is shifted to 458 cm^{-1} and the shape becomes broad and asymmetrical. This position shift is related to the enlarged lattice space because of the smaller size of ceria crystals (3.5 nm), since the Raman peak's position varies with the change of the interatomic force which is characterized by the change of bond length, as well as the change of the lattice spacing. The relationship between the Raman shift and the change of the lattice parameter can be expressed by the following equation:

$$\Delta\omega = -3\gamma\omega_0\Delta a/a_0$$

where ω_0 is Raman frequency of bulk CeO_2, a_0 is the CeO_2 lattice constant (0.5411 nm), Δa is the change in lattice constant, and γ is the Grüneisen constant with a value of 1.24.[31a] In our experiment the calculated Raman frequency shift $\Delta\omega$ is -6.06 cm^{-1}, which is very close to the experimental frequency shift of -6 cm^{-1}. Besides the peak at 458 cm^{-1}, two weak second-order peaks appear at around 261 and 600 cm^{-1}. The former is assigned to the transverse acoustic (TA) mode[32] and the latter to the nondegenerate longitudinal optical (LO) mode because of the presence of defects which results from the formation of oxygen vacancies.[32,31a] The existence of oxygen vacancies is especially important to enhance the activity of the oxygen ions for catalytic reactions. Meanwhile, the peak for the $^2F_{5/2}$ to $^2F_{7/2}$ electronic transition of Ce(III) at around 2100 cm^{-1} is not observed (Supporting Information, Figure S1), signifying that there is no apparent Ce(III) species and thus no luminescence of rare earth impurities that could influence the observed Raman spectra.[33] Therefore, the results of the Raman spectroscopy further confirm the characteristics of small-sized ceria nanocrystals packed in the spherical aggregates, which is in agreement with the results deduced from XRD, TEM, XPS, and UV−vis absorption analysis.

CeO_2 is an important three-way catalyst used in automobile exhaust systems,[1a,b] and these catalysts, loaded with noble metals (Au, Pt, Pd, and Rh), exhibit high catalytic activity.[5,34] In recent years, much research has been focused on ceria-based transition metal catalysts, instead of the costly noble metal.[35] Figure 12 shows the catalytic activity profiles of the spherical aggregates and mesoporous CeO_2 loaded with 5 wt % CuO. It is noted that the CO conversion increases with the promotion of the reaction temperature, and 100% conversion rate is achieved at a low-temperature of 150 °C, indicating high catalytic activities of both the $CuO-CeO_2$ catalysts. The high catalytic activities are attributed to the reversible $CeO_2-Ce_2O_3$ transition in CeO_2 support with intrinsically small crystallite size. It is noted that the two samples exhibit similar high catalytic activities due to the annealing process at 500 °C which is conducive to crystallization, sintering, and growth of the CeO_2 nanocrystals. Therefore, the differences in morphology (Supporting Information, Figure S2) and BET surface area (26 and 41 m^2/g, respectively) of the samples are reduced. Furthermore, it is believed that the high catalytic activity of the CeO_2-based materials also stemmed from the high oxygen-vacancy formation and migration. The CO_2 is a potential oxidant capable to fill-in oxygen vacancies of ceria via reactions: $2Ce_{Ce}^X + O_O^X \rightarrow 2Ce'_{Ce} + V_{\ddot{O}} + \frac{1}{2}O_2(g)$, $CO(g) + \frac{1}{2}O_2(g) \rightarrow CO_2(g)$, where Ce_{Ce}^X denotes the cerium in the lattice of CeO_2, O_O^X denotes the

Nearly Monodisperse Spherical Aggregates

J. Phys. Chem. C, Vol. 112, No. 47, 2008 **18411**

oxygen in the lattice of CeO_2, and Ce'_{Ce} denotes a Ce^{3+} that occupies the site normally occupied by a Ce^{4+} because of the transformation from Ce^{4+} to Ce^{3+}, and $V_{\ddot{O}}$ represents the O^{2-} vacancy produced by the release of O_2.[36] Therefore, the high oxygen-vacancy formation in this system, evidenced by Raman analysis, may be crucial to the observed excellent catalytic activity.[37]

Conclusions

In summary, we have developed a sustainable and facile method to produce nearly monodisperse spherical aggregates of CeO_2 nanocrystals, which involves the use of the ionic liquid as both template and solvent. The spherical aggregates, with average diameter of 100−150 nm, are composed of ca. 3.5 nm CeO_2 nanocrystals as building units, giving rise to a 3D open porous structure with a high BET surface area of 119 $m^2 \cdot g^{-1}$. Tuning the amount of the ILs in the synthesis allows for the preparation of mesoporous CeO_2 with a surface area up to 227 $m^2 \cdot g^{-1}$. Loaded with 5 wt% CuO, both the spherical aggregates and mesoporous CeO_2 functional materials exhibit high catalytic activities for CO conversion with 100% conversion rate at a low temperature of 150 °C, suggesting potential applications in automobile emission control and other catalytic reactions. This facile method would be a general way to fabricate a 3D nanostructure composed of small-sized building blocks. That is, this work provides a new approach to fabricate the sub-microsized CeO_2 aggregates with the characteristics of CeO_2 nanocrystals. We believe that it is very useful for the manipulation of nanocrystals and further benefits real application in practice.

Supporting Information Available: Full Raman spectra of the spherical aggregates CeO_2 (Figure S1); TEM images of spherical aggregates and mesoporous CuO−CeO_2 catalyst annealed at 500 °C (Figure S2). This material is available free of charge via the Internet at http://pubs.acs.org.

References and Notes

(1) (a) Kašpar, J.; Fornasiero, P.; Graziani, M. *Catal. Today* **1999**, *50*, 285. (b) Kašpar, J.; Fornasiero, P.; Hickey, N. *Catal. Today* **2003**, *77*, 419. (c) Si, R.; Zhang, Y. W.; Li, S. J.; Lin, B. X.; Yan, C. H. *J. Phys. Chem. B* **2004**, *108*, 12481. (d) Masui, T.; Fujiwara, K.; Machida, K. I.; Adachi, G. Y. *Chem. Mater.* **1997**, *9*, 2197. (e) Steele, B. C. H. *Nature* **1999**, *400*, 619. (f) Tye, L.; El-Masry, N. A.; Chikyowm, T.; McLarty, P.; Bedair, S. M. *Appl. Phys. Lett.* **1994**, *65*, 3081. (g) Lee, S. H.; Lu, Z. Y.; Babu, S. V.; Matijevic, E. *J. Mater. Res.* **2002**, *17*, 2744. (h) Beie, H. J.; Gnoerich, A. *Sens. Actuators B* **1991**, *4*, 393. (i) Corma, A.; Atienzar, P.; Garcia, H.; Chane-Ching, J. Y. *Nat. Mater.* **2004**, *3*, 394.

(2) Ho, C. M.; Yu, J. C.; Kwong, T.; Mak, A. C.; Lai, S. *Chem. Mater.* **2005**, *17*, 4514.

(3) Zhou, K. B.; Wang, X.; Sun, X. M.; Peng, Q.; Li, Y. D. *J. Catal.* **2005**, *229*, 206.

(4) Zhang, Y. W.; Si, R.; Liao, C. S.; Yan, C. H.; Xiao, C. X.; Kou, Y. *J. Phys. Chem. B* **2003**, *107*, 10159.

(5) Si, R.; Flytzani-Stephanopoulos, M. *Angew. Chem., Int. Ed.* **2008**, *47*, 2884.

(6) Lu, A. H.; Spliethoff, B.; Schüth, F. *Chem. Mater.* **2008**, *20*, 5314.

(7) Boettcher, S. W.; Fan, J.; Tsung, C.; Shi, Q.; Stucky, G. D. *Acc. Chem. Res.* **2007**, *40*, 784.

(8) Laberty-Robert, C.; Long, J. W.; Lucas, E. M.; Pettigrew, K. A.; Stroud, R. M.; Doescher, M. S.; Rolison, D. R. *Chem. Mater.* **2006**, *18*, 50.

(9) Hirano, M.; Inagaki, M. *J. Mater. Chem.* **2000**, *10*, 473.

(10) Gesser, H. D.; Goswami, P. C. *Chem. Rev.* **1989**, *89*, 765.

(11) Masui, T.; Fujiwara, K.; Machida, K.; Adachi, G.; Sakata, T.; Mori, H. *Chem. Mater.* **1997**, *9*, 2197.

(12) Pijolat, M.; Viricelle, J. P.; Sosutelle, M. *Stud. Surf. Sci. Catal.* **1997**, *91*, 885.

(13) Purohit, R. D.; Sharma, D.; Pillai, K. T.; Tyagi, A. K. *Mater. Res. Bull.* **2001**, *36*, 2711.

(14) Pan, C. S.; Zhang, D. S.; Shi, L. Y.; Fang, J. H. *Eur. J. Inorg. Chem.* **2008**, 2429.

(15) Pan, C. S.; Zhang, D. S.; Shi, L. Y. *J. Solid State Chem.* **2008**, *181*, 1298.

(16) Zhang, D. S.; Huang, L.; Zhang, J. P.; Shi, L. Y. *J. Mater. Sci.* **2008**, *43*, 5647.

(17) Zhang, D. S.; Fu, H. X.; Shi, L. Y.; Fang, J. H.; Li, Q. *J. Solid State Chem.* **2007**, *180*, 654.

(18) (a) Zhou, Y.; Antonietti, M. *J. Am. Chem. Soc.* **2003**, *125*, 14960. (b) Fonseca, G. S.; Umpierre, A. P.; Fichtner, P. F. P.; Teixeira, S. R.; Dupont, J. *Chem. Eur. J.* **2003**, *9*, 3263. (c) Antonietti, M.; Kuang, D.; Smarsly, B.; Zhou, Y. *Angew. Chem., Int. Ed.* **2004**, *43*, 4988. (d) Zhou, Y.; Schattka, J. H.; Antonietti, M. *Nano Lett.* **2004**, *4*, 477. (e) Zhou, Y.; Antonietti, M. *Adv. Mater.* **2003**, *15*, 1452. (f) Zhou, Y.; Antonietti, M. *Chem. Mater.* **2004**, *16*, 544. (g) Park, H.; Yang, S. H.; Jun, Y.; Hong, W. H.; Kang, J. K. *Chem. Mater.* **2007**, *19*, 535.

(19) (a) Deshmukh, R. R.; Rajagopal, R.; Srinivasan, K. V. *Chem. Commun.* **2001**, 1544. (b) Dupont, J.; Fonseca, G. S.; Umpierre, A. P.; Fichtner, P. F. P.; Teixeira, S. R. *J. Am. Chem. Soc.* **2002**, *124*, 4228. (c) Endres, F.; El Abedin, S. Z. *Chem. Commun.* **2002**, 892. (d) Nakashima, T.; Kimizuka, N. *J. Am. Chem. Soc.* **2003**, *125*, 6386. (e) Ding, K.; Miao, Z.; Liu, Z.; Zhang, Z.; Han, B.; An, G.; Miao, S.; Xie, Y. *J. Am. Chem. Soc.* **2007**, *129*, 6362. (f) Parnham, E. R.; Morris, R. E. *Acc. Chem. Res.* **2007**, *40*, 1005.

(20) Itoh, H.; Naka, K.; Chujo, Y. *J. Am. Chem. Soc.* **2004**, *126*, 3026.

(21) Zhu, Y. J.; Wang, W. W.; Qi, R. J.; Hu, X. L. *Angew. Chem., Int. Ed.* **2004**, *43*, 1410.

(22) (a) Cooper, E. R.; Andrews, C. D.; Wheatley, P. S.; Webb, P. B.; Wormald, P.; Morris, R. E. *Nature* **2004**, *430*, 1012. (b) Parnham, E. R.; Morris, R. E. *Chem. Mater.* **2006**, *18*, 4882. (c) Parnham, E. R.; Morris, R. E. *J. Am. Chem. Soc.* **2006**, *128*, 2204.

(23) (a) Liu, D. P.; Li, G. D.; Su, Y.; Chen, J. S. *Angew. Chem., Int. Ed.* **2006**, *45*, 7370. (b) Liu, D. P.; Li, G. D.; Li, J. X.; Li, X. H.; Chen, J. S. *Chem. Commun.* **2007**, 4131.

(24) (a) Qian, L.; Yang, X. R. *J. Phys. Chem. B* **2006**, *110*, 16672. (b) Zhou, H. P.; Zhang, Y. W.; Mai, H. X.; Sun, X.; Liu, Q.; Song, W. G.; Yan, C. H. *Chem. Eur. J.* **2008**, *14*, 3380.

(25) Gregg, S. J.; Sing, K. S. W. *Adsorption, Surface Area and Porosity*; Academic: London, 1997.

(26) Dai, S.; Ju, Y. H.; Gao, H. J.; Lin, J. S.; Pennycook, S. J.; Barnes, C. E. *Chem. Commun.* **2000**, 243.

(27) Fitchett, B. D.; Conboy, J. C. *J. Phys. Chem. B* **2004**, *108*, 20255.

(28) (a) Pfau, A.; Schierbaum, K. D. *Surf. Sci.* **1994**, *321*, 71. (b) Shyu, J. Z.; Optto, K.; Watkins, W. L. H.; Graham, G. W.; Belitz, R. K.; Gandhi, H. S. *J. Catal.* **1988**, *114*, 23. (c) Fujimori, A. *Phys. Rev. B* **1983**, *28*, 2281.

(29) (a) Marabelli, F.; Wachter, P. *Phys. Rev. B* **1987**, *36*, 1238. (b) Petrovsky, V.; Gorman, B. P.; erson, H. U.; Petrovsky, T. *J. Appl. Phys.* **2001**, *90*, 2517. (c) Hernandez-Alonso, M. D.; Hungria, A. B.; Martinez-Arias, A. J.; Coronado, M. *Phys. Chem. Chem. Phys.* **2004**, *6*, 3524. (d) Tsunekawa, S.; Fukuda, T.; Kasuya, A. *J. Appl. Phys.* **2000**, *87*, 1318. (e) Patsalas, P.; Logothetidis, S. *Phys. Rev. B* **2003**, *68*, 035104.

(30) Welton, T. *Chem. Rev.* **1999**, *99*, 2071.

(31) (a) McBride, J. R.; Hass, K. C.; Poindexter, B. D.; Weber, W. H. *J. Appl. Phys.* **1994**, *76*, 2435. (b) Lin, X. M.; Li, L. P.; Li, G. S.; Su, W. H. *Mater. Chem. Phys.* **2001**, *69*, 236.

(32) Spanier, J. E.; Robinson, R. D.; Zhang, F.; Chan, S. W.; Herman, I. P. *Phys. Rev. B* **2001**, *64*, 245407.

(33) (a) Fornasiero, P.; Speghini, A.; Monte, R. D.; Bettinelli, M.; Kašpar, J.; Bigotto, A.; Sergo, V.; Graziani, M. *Chem. Mater.* **2004**, *16*, 1938. (b) Otake, T.; Yugami, H.; Naito, H.; Kawamura, K.; Kawada, T.; Mizusaki, J. *Solid State Ionics* **2000**, *135*, 663.

(34) (a) Zhu, H. Q.; Qin, Z. F.; Shan, W. J.; Shen, W. J.; Wang, J. G. *J. Catal.* **2004**, *225*, 267. (b) Budroni, G.; Corma, A. *Angew. Chem., Int. Ed.* **2006**, *45*, 3328. (c) Fu, Q.; Weber, A.; Flytzani-Stephanopoulos, M. *Catal. Lett.* **2001**, *77*, 87. (d) Yeung, C. M. Y.; Yu, K. M. K.; Fu, Q. J.; Thompsett, D.; Petch, M. I.; Tsang, S. C. *J. Am. Chem. Soc.* **2005**, *127*, 18010. (e) Huang, P. X.; Wu, F.; Zhu, B. L.; Gao, X. P.; Zhu, H. Y.; Yan, T. Y.; Huang, W. P.; Wu, S. H.; Song, D. Y. *J. Phys. Chem. B* **2005**, *109*, 19169.

(35) (a) Wang, J. B.; Tsai, D. H.; Huang, T. J. *J. Catal.* **2002**, *208*, 370. (b) Martínez-Arias, A.; Hungria, A. B.; Fernández-García, M.; Conesa, J. C.; Munuera, G. *J. Phys. Chem. B* **2004**, *108*, 17983. (c) Avgouropoulos, G.; Ioannides, T. *Appl. Catal., A* **2003**, *244*, 155.

(36) Trovarelli, A. *Catalysis by Ceria and Related Materials*, 2nd ed.; Dunod: London, 2002.

(37) Skorodumova, N. V.; Simak, S. I.; Lundqvist, B. I.; Abrikosov, I. A.; Johansson, B. *Phys. Rev. Lett.* **2002**, *89*, 166601.